ACS SyntheticBiology
Research Article
Cite This: ACS Synth. Biol. 2019, 8, 807−817
pubs.acs.org/synthbio

Combinatorial Sensor Design in *Caulobacter crescentus* for Selective Environmental Uranium Detection

Dan M. Park*,† and Michael J. Taffet‡

†Biosciences and Biotechnology Division, Physical and Life Sciences Directorate, Lawrence Livermore National Laboratory, Livermore, California 94550, United States

‡Environmental Restoration Department (ERD), Operations and Business Directorate, Lawrence Livermore National Laboratory, Livermore, California 94550, United States

Supporting Information

ABSTRACT: The ability to detect uranium (U) through environmental monitoring is of critical importance for informing water resource protection and nonproliferation efforts. While technologies exist for environmental U detection, wide-area environmental monitoring, i.e. sampling coverage over large areas not known to possess U contamination, remains a challenging prospect that necessitates the development of novel detection approaches. Herein, we describe the development of a whole-cell U sensor by integrating two functionally independent, native U-responsive two-component signaling systems (TCS), UzcRS and UrpRS, within an AND gate circuit in the bacterium *Caulobacter crescentus*. Through leverage of the distinct but imperfect selectivity profiles of both TCS, this combinatorial approach enabled greater selectivity relative to a prior biosensor developed with UzcRS alone; no cross-reactivity was observed with most common environmental metals (e.g, Fe, As, Cu, Ca, Mg, Cd, Cr, Al) or the U decay-chain product Th, and the selectivity against Zn and Pb was significantly improved. In addition, integration of the UzcRS signal amplifier protein UzcY within the AND gate circuit further enhanced overall sensitivity and selectivity for U. The functionality of the sensor in an environmental context was confirmed by detection of U concentrations as low as 1 μM in groundwater samples. The results highlight the value of a combinatorial approach for constructing whole-cell sensors for the selective detection of analytes for which there are no known evolved regulators.

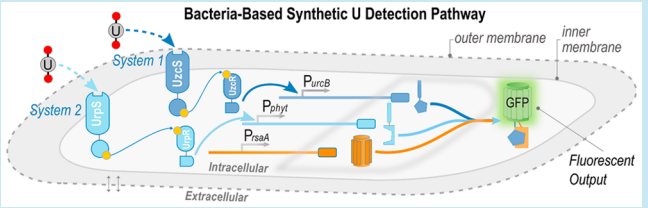

KEYWORDS: *two-component system, whole-cell sensor, uranium, uranium sensor, combinatorial sensor*

INTRODUCTION

Uranium is a highly abundant naturally occurring radionuclide that has been heavily mined and processed over the last several decades for nuclear energy and weapons production. As a consequence of regular and accidental discharges of waste and effluent during the nuclear fuel cycle, significant quantities of U have been disseminated into the environment.[1] U is toxic as both a radioisotope and a heavy metal with exposure associated with nephrotoxicity, genotoxicity, reproductive defects, and diminished bone growth.[2] Accordingly, the US Environmental Protection Agency (EPA) has established a maximum contaminant level (MCL) of 30 ppb (~130 nM) for U in drinking water. However, groundwater concentrations in the United States and worldwide frequently exceed this limit, even in regions lacking U mining/enrichment activities, and may occur wholly as natural background.[3−5] To minimize human exposure, motivate environmental cleanup efforts, and enhance nonproliferation efforts, it is imperative that environmental U concentrations are monitored in a robust, cost-effective, and *in situ* manner. An *in situ* system would enable rapid detection and notification, ensuring that a release of U into groundwater would be recognized and met with a rapid response to protect impacted water resources.

Established technologies for U detection have limitations that hinder wide area *in situ* monitoring. Typically, environmental U detection involves in-field sample collection (e.g., from a pumped or bailed water sample)), followed by sample preparation and analytical quantification in the laboratory using mass spectrometry (e.g., ICP-MS, SIMS, FT-TIMs).[6] While sensitive and selective, these technologies are equipment-intensive, costly, require skillful operation, and cannot be easily applied for *in situ* sampling, greatly limiting sampling throughput.

Compared to traditional U detection technologies, whole-cell biosensors[7,8] have intrinsic advantages that are beneficial to the development of remote detection or wide-area environmental monitoring methodologies, including rapid real time detection of release of U to groundwater. Microorganisms offer the potential for cost-effective, potentially autonomous detection functionality because the necessary macromolecular components for analyte detection would be synthesized as a function of the organism's developmental lifecycle. Past efforts using single input whole-cell biosensors have demonstrated promising

Received: November 21, 2018
Published: March 21, 2019

DOI: 10.1021/acssynbio.8b00484
ACS Synth. Biol. 2019, 8, 807−817

results within the sectors of heavy/semimetal detection in aqueous systems,[7−10] pathogen detection and eradication,[11] organic pollutant detection,[12] and standoff detection of landmines.[13,14] However, unlike these sensors that leverage regulators that, in most cases, have evolved for the selective detection of the compound of interest, the construction of a whole-cell sensor of U has been hindered by the absence of characterized U-specific sensing systems.

Attempts to engineer a macromolecular U-sensing functionality have yielded promising results but require further development for whole-cell sensor application. DNAzymes[15,16] and antibodies[17] that bind with high affinity and specificity the uranyl oxycation and a U(VI) chelate complex, respectively, have been selected through screening. While both systems enabled robust *in vitro* U detection platforms,[15,16,18] it is unclear how either could be implemented *in vivo*. Additionally, the nickel-coordination site of the NikR transcriptional repressor was rationally engineered to selectivity coordinate the uranyl oxycation (UO_2^{2+}), enabling U-dependent DNA binding *in vitro*;[19] however, the efficacy of this sensor *in vivo* has yet to be determined. Another potential avenue to improve U biosensor selectivity is through the design of synthetic genetic logic circuits that incorporate multiple sensory inputs (e.g., an AND gate approach).[9,20,21] For example, a selective Zn-sensing AND gate was constructed by integrating regulatory input from two Zn-responsive promoters (P_{zntA} and P_{zraP}), which individually exhibit imperfect but distinct selectivity profiles.[20] Additionally, work by Clarke et al. suggests that a combinatorial sensor approach using multiple regulators with broad specificity profiles could be adopted for the selective detection of compounds lacking specific regulators (e.g., butanol).[22] To apply this combinatorial input logic toward U detection, we developed an AND gate circuit by integrating two functionally independent, native U-responsive regulatory pathways into a single synthetic pathway in *Caulobacter crescentus*.

Prior studies revealed that *C. crescentus* tolerates high U concentrations relative to other model bacteria[23,24] and exhibits a robust gene expression response following U exposure, which includes numerous genes of unknown function.[23,25,26] Using the promoter of the highest U-induced gene, *urcA* (P_{urcA}), to drive expression of UV-excitable *gfp*, Hillson et al. generated a whole-cell U sensor that was responsive to submicromolar U concentrations and successfully detected U in a groundwater sample.[26] Subsequent genetic and biochemical analyses revealed that the majority of U-dependent gene induction in this bacterium, including regulation of P_{urcA}, is mediated by the TCS UzcRS, supporting a role for UzcRS as a U-responsive master regulator.[27] However, characterization of the specificity of UzcRS revealed strong cross-reactivity with the common environmental metals Zn and Cu.[27] To generate a U sensor with improved selectivity relative to UzcRS, we identified and characterized the selectivity of a second U-responsive regulatory system (UrpRS) in *C. crescentus*. Leveraging the distinct selectivity profiles of UzcRS and UrpRS and the tripartite GFP genetic framework,[28] an AND gate circuit that integrates signaling input from both pathways was constructed and characterized.

RESULTS AND DISCUSSION

Identification of the U-Responsive UrpRS TCS. Examination of U and Zn transcriptomic data[23,27] *in C. crescentus* revealed a small subset of highly U-induced genes that are not regulated by UzcRS and only weakly induced by Zn (Figure S1A). Two operons (CCNA_01361-CCNA_01362-CCNA_01363 and CCNA_01353-CCNA_01352-CCNA_01351) were of particular interest based on several observations. First, both operons are highly induced by U in minimal and complex media but lack induction by other known stress responses (e.g., DNA damage, heat shock, heavy metals; Table S1). The operons are furthermore likely regulated by the same transcription factor based on the presence of nearly identical DNA sites comprised of two tandem direct repeats (5′-GTCAG-3′; Figure 1A) with 11-bp center-to-center (ctc) spacing within the CCNA_01353 (P_{phyt}) and CCNA_01361 promoters (P_{1361}). This direct repeat site is conserved within the promoters of closely related alpha proteobacteria (Figure 1B) and required for U-dependent induction of P_{phyt} and P_{1361}; mutations away from consensus in both P_{phyt}- and P_{1361}-*gfp* fusions abrogated U-induction (Figure S1B and C). The CCNA_01353-CCNA_01352-CCNA_01351 operon encodes a phytase enzyme that confers U tolerance[25] and an uncharacterized response regulator and histidine kinase pair, while the CCNA_01361-CCNA_01362-CCNA_01363 operon encodes a PepSY superfamily protein and another uncharacterized response regulator and histidine kinase pair.

This direct repeat binding site bears striking resemblance to the binding sites of OmpR/PhoB family response regulators.[29,30] As such, the OmpR/PhoB-family response regulators CCNA_01351 and CCNA_01362, whose expression is governed by P_{phyt} and P_{1361}, respectively, are potential candidates for the U-responsive regulator. Deletion of CCNA_01351 or the histidine kinase CCNA_01352 had no effect on U-dependent induction of either promoter (data not shown), consistent with the results of transcriptomics performed with both mutants during U exposure.[23] In contrast, deletion of CCNA_01362 or the histidine kinase CCNA_01363 abolished U-dependent induction of both promoters (Figure 1C). Furthermore, a forward genetic screen for mutants that failed to induce P_{phyt}-*lacZ* in response to U resulted in five transposons that mapped to unique locations within CCNA_01362 and CCNA_01363 (Figure S2; Table S2), providing independent validation for a functional role of both proteins in U-dependent stimulation of P_{phyt}. We tentatively named these proteins UrpR and UrpS (uranium responsive phytase regulator and sensor, respectively) because this TCS strongly activates a gene encoding a phytase enzyme.

To confirm that regulation by UrpR is direct, UrpR was purified, and its binding to P_{phyt} was tested using an electrophoretic mobility shift assay. As expected, UrpR bound to P_{phyt} in a concentration-dependent manner (Figure 1D). Binding was not observed to a P_{phyt} fragment containing a 5′-GTCA-3′ to 5′-CAGT-3′ mutation at DR2 (Figure 1D), supporting the functional role of the direct repeat site in UrpR DNA binding. Collectively, these data suggest that the TCS comprised of UrpR and UrpS is the U-dependent activator of P_{phyt} and P_{1361}, revealing a positive feedback loop within this regulatory system.

UrpRS Exhibits Improved Metal Selectivity Compared to UzcRS. To test whether UrpRS functions independently of UzcRS with respect to U perception (a property that is important for its dual integration with UzcR in a synthetic U sensing pathway), the expression of P_{phyt} and the UzcR-regulated promoter P_{urcB} were tested in strains lacking the noncognate TCS. The U-induction profile of a shortened P_{phyt} reporter ($P_{phyt\text{-}short}$; diagrammed in Figure 1A) was largely unaffected by deletion of *uzcR* or *uzcS* (Figure 2A; Figure S3A),

DOI: 10.1021/acssynbio.8b00484
ACS Synth. Biol. 2019, 8, 807−817

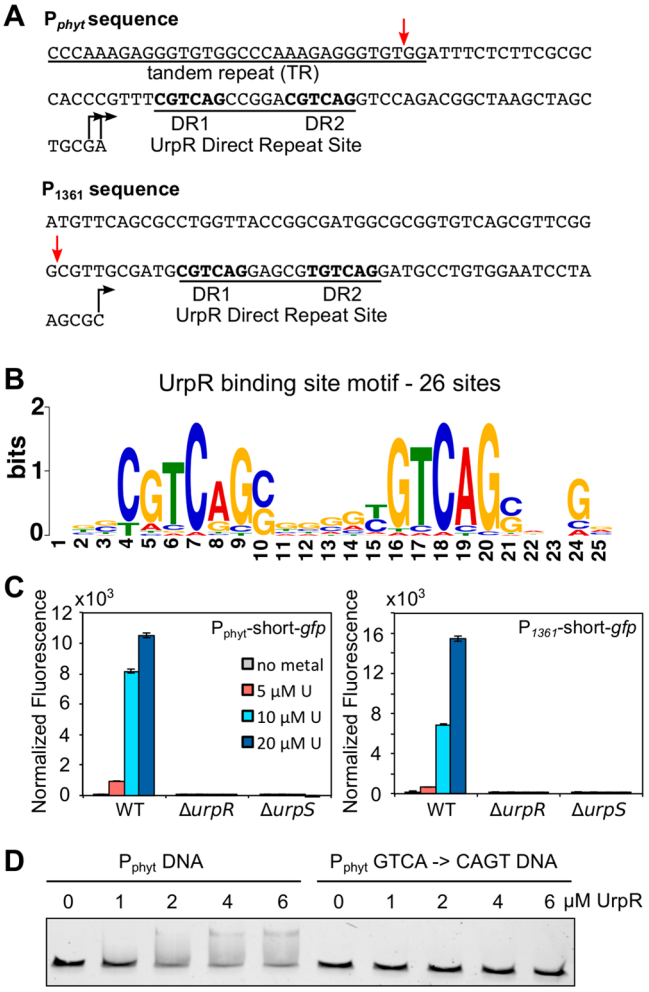

Figure 1. Identification of the U-responsive TCS UrpRS. (A) Depiction of the P_{phyt} and P_{1361} promoter sequences with the U-responsive regulator binding site underlined. Black arrows represent putative transcription start sites based on RNA-seq data (D. Park, unpublished experiments), and the red arrow depicts the 5′ end of each shortened promoter sequence. A large tandem repeat (TR) in P_{phyt} that is not required for U-dependent regulation (Figure S1B) is denoted by an underline. (B) A phylogenetic footprinting approach was used to construct a DNA-binding motif for the P_{phyt}/P_{1361} regulator (UrpR). An alignment of 26 P_{phyt} or P_{1361} DNA sequences from the subclass Caulobacteridae, Bradyrhizobiaceae, Sphingomonadaceae, Hyphomicrobiaceae, and Rhodobacteracea are indicated, with larger letters representing a higher level of consensus between aligned sequences. (C) The fluorescence of shortened P_{phyt}-*gfp* and P_{1361}-*gfp* reporters was quantified following a two-hour exposure of wild-type *C. crescentus* and strains deleted for *urpR* (CCNA_01362) and *urpS* (CCNA_01363). Error bars represent the standard deviation of triplicates. (D) EMSA of UrpR binding to wild-type and mutant P_{phyt} fragments. The mutant P_{phyt} DNA contains a GTCA → CAGT mutation of DR2 (see panel A). The assays were performed with 50 nM 6-FAM-labeled DNA and UrpR, phosphorylated with carbamoyl phosphate. The concentrations indicate the total UrpR used in the assay. A representative example of three biological replicates is depicted.

while the U-induction profile for P_{urcB}-*gfp* was unaffected by deletion of *urpR or urpS* (Figure 2A; Figure S3A). Collectively, these data indicate that *C. crescentus* possesses at least two independent U-responsive TCS.

To determine the metal selectivity of UrpRS, $P_{phyt\text{-}short}$-*gfp* fluorescence was quantified following exposure to 16 metals of environmental relevance (Figure 2B). To encourage metal solubility and thus bioavailability, we employed minimal media containing glycerol-2-phosphate (G2P) as the sole source of phosphate. As a control, the metal selectivity of the P_{urcB}-*gfp* reporter was also tested (Figure 2C). For both promoters, the strongest induction was observed in response to U; however, $P_{phyt\text{-}short}$ exhibited greater U sensitivity, resembling a switch-like activation response (Figure 2A) that can likely be attributed to the strong positive autoregulation within the UrpRS system. Most metals, including Th, a radionuclide that is part of the U decay chain and often co-occurs with U, failed to induce either reporter (Table S3). Importantly, $P_{phyt\text{-}short}$ was unresponsive to Cu and only minimally responsive to Zn or Pb (Figure 2B). In contrast, strong P_{urcB} induction was observed with Zn, Pb, and within a narrow Cu concentration range (Figure 2C). This narrow responsiveness to Cu reflects its high toxicity in minimal media.[27] The Pb-dependent induction of P_{urcB} was surprising and contrasts with prior reports.[26,27] We suspect that the Pb induction likely reflects the higher initial Pb bioavailability in the presence of G2P compared to orthophosphate, given the low solubility of lead phosphate.[31] These data suggest that while UrpRS is not exclusively selective for U, it exhibits an improved metal selectivity profile compared to UzcRS.

Construction of a U-Responsive AND Gate Pathway in *C. crescentus*. Given the distinct metal selectivity profiles and functional independence of UzcRS and UrpRS, we hypothesized that a combinatorial approach that incorporates the U-responsive functionality of both UrpRS and UzcRS will yield a whole-cell U sensor with enhanced specificity. Accordingly, the recently developed Tripartite GFP system[28] was used as a template to construct a U sensing AND gate. In this system, GFP is split into three parts (gfp10, gfp11, and gfp1−9) that interact to reconstitute active GFP when coexpressed; the synthetic K1 and E1 coiled-coils[32] were fused to the C-terminus of gfp10 and the N-terminus of gfp11, respectively, to mediate dimerization.[28] An advantage of the tripartite system is the low basal level of GFP fluorescence, ensuring a robust OFF state. $P_{phyt\text{-}short}$ and P_{urcB}, which both exhibit low basal activity and a large U-dependent fold change, were used to drive expression of *gfp10-K1* and *E1-gfp11*, respectively. The expression of *gfp1−9* was driven by the strong, constitutive *rsaA* promoter (P_{rsaA})[33] to produce high GFP1−9 levels at all stages of growth (Figure 3A; diagrammed in Figure S4). Hereafter, we refer to this sensor configuration in an otherwise wild-type (WT) strain background as the core sensor. Sensor variants where *gfp1−9* expression was driven by the xylose-inducible promoter (P_{xyl})[34] or the UrpR-regulated P_{phyt} were also tested but exhibited a lower signal amplitude and were not pursued further (Figure S5A and B).

Initial characterization of the tripartite U sensor was performed in M5G G2P, given the robust U-dependent induction of both P_{phyt} and P_{urcB} under these conditions and the lack of induction in growth media containing orthophosphate, where U bioavailability is low as a result of uranyl phosphate mineralization.[24,35] Notably, the basal fluorescence output of the sensor was indistinguishable from a control strain lacking GFP1−9 expression, supporting a very low OFF state (Figure 3B). Addition of uranyl nitrate, but not nitrate alone (Figure S6), yielded a nonlinear fluorescence response curve that deviated from background at concentrations as low as 5 μM and plateaued at ∼15 μM (Figure 3B). The hypersensitivity of the U response curve was quantified by fitting the data with a Hill function. We note that this approach is semiempirical and is not used as a basis to derive insight on the mechanisms of the

DOI: 10.1021/acssynbio.8b00484
ACS Synth. Biol. 2019, 8, 807−817

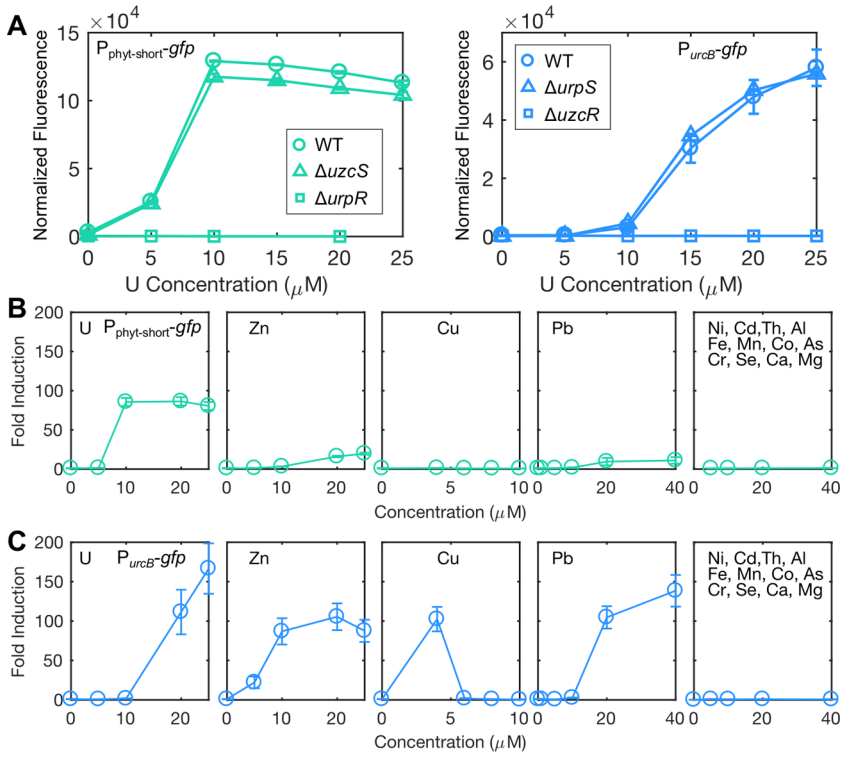

Figure 2. Metal selectivity of UrpRS and UzcRS. (A) Functional independence of UrpRS and UzcRS. U response curves of $P_{phyt\text{-}short}$-*gfp* and P_{urcB}-*gfp* reporters were determined by quantifying fluorescence following a 2 h exposure to a range of U concentrations in wild-type *C. crescentus* and strains deleted for *uzcS*, *urpS*, and the cognate response regulator. Error bars represent the standard deviation of biological triplicates. Metal selectivity profiles for $P_{phyt\text{-}short}$-*gfp* (panel B) and P_{urcB}-*gfp* (panel C). Reporter fluorescence was quantified following a 2 h exposure to 16 metals. The furthest right plot depicts representative data for metals that failed to induce either promoter. For reference, the fold induction values can be found in Table S3, and the normalized fluorescence data for panels B and C are plotted in Figure S3B. Error bars represent the standard deviation of biological triplicates.

reactions occurring in the system. The model revealed a hill coefficient (n^H) of 7.6 and a half maximal fluorescence response (K) at 9.9 μM U (Table 1). The hypersensitive nature of the U response curve suggests that the core sensor is well-poised as a qualitative YES/NO digital sensor of environmental U.

Importantly, U-dependent fluorescence was not observed with control sensor variants that lacked either a functional UrpR binding site in $P_{phyt\text{-}short}$ or *gfp1−9* expression (Figure 3B). Additionally, deletion of *uzcR* severely impaired, but did not completely abolish, U-dependent fluorescence (Figure 3B). Because the data in Figure 2A indicate that P_{urcB} activity is negated by *uzcR* deletion, the minor induction of sensor fluorescence in the Δ*uzcR* strain may reflect low-level transcriptional read-through of the transcription terminator separating $P_{phyt\text{-}short}$-*gfp10-K1* and P_{urcB}-*E1-gfp11* modules (diagramed in Figure S4). Collectively, these data highlight the requirement for expression from all three promoters for a U-dependent fluorescent output.

U-Sensing AND Gate Exhibits Improved Selectivity Relative to UzcRS Alone. To characterize the selectivity of the core sensor, fluorescence was quantified in response to known inducers of either TCS and compared to results obtained with control sensor variants where either UzcRS or UrpRS governs the expression of both *gfp10* and *gfp11* (Figure 4; diagrammed in Figure S4). Consistent with the U response curves for $P_{phyt\text{-}short}$- and P_{urcB}-gfp fusions (Figure 2A), the control sensor driven by UrpRS alone yielded a U response curve with greater sensitivity compared to the sensor driven by UzcRS alone (n^H of 12.5, K of 8.8 μM compared to n^H of 7.9 and K of 17.4 μM; Table 1; Figure S7). As expected, the core sensor was unresponsive to Ni, Cd, Th, Al, Fe(III), Fe(II), Mn, Co, arsenate, Se, and chromate (Figure S8). The core sensor and the sensor variant driven by UrpRS alone were also unresponsive to Cu, in contrast to the sensor driven exclusively by UzcRS (Figure 4). Critically, the sensitivity of the core sensor to Zn and Pb was significantly diminished relative to the UzcRS control; Pb concentrations greater than 20 μM, which are unlikely to be encountered in surface or groundwater,[36,37] were required for weak fluorescence induction, while the Zn-induced fluorescence was reduced relative to U for every tested concentration. Despite the improved selectivity for U, low Zn concentrations (5 μM Zn) yielded a fluorescence response in the core sensor that exceeded the U response at this same concentration (Figure S9A). Nevertheless, the lack of Cu responsiveness and the weakened Zn/Pb responsiveness of the core sensor relative to a sensor constructed with UzcRS alone highlights the selectivity improvement of the AND gate approach.

Integration of UzcY Signal Amplifier Improves U Sensitivity and Selectivity. A notable limitation of this AND gate approach is that the improved selectivity comes at a cost to U sensitivity in the low micromolar range; incorporation of the less sensitive UzcRS TCS yielded a sensor with lower sensitivity compared to the control sensor driven by UrpRS alone (Figure S7). Notably, swapping the UzcRS-regulated P_{urcB} promoter with P_{urcA}, the highest induced UzcR promoter,[27] failed to significantly improve sensor sensitivity (data not shown). This suggests that simply swapping P_{urcB} with an alternative UzcR-regulated promoter is unlikely to remedy the sensitivity limitation.

DOI: 10.1021/acssynbio.8b00484
ACS Synth. Biol. 2019, 8, 807−817

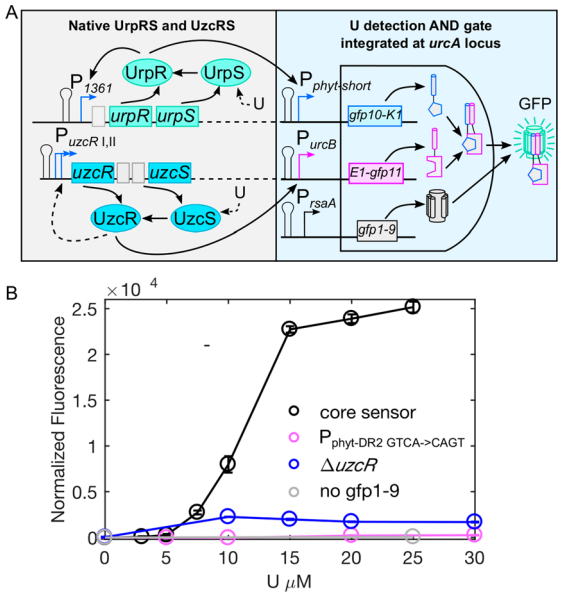

Figure 3. U-responsive AND gate design. (A) Schematic of a U-responsive AND gate (core sensor) that utilizes the tripartite GFP system[28] in which *gfp10* is placed under the control of $P_{phyt\text{-}short}$, *gfp11* is placed under the control of P_{urcB}, and *gfp1–9* is placed under the control of the *Caulobacter* S-layer promoter, P_{rsaA}, which is a strong, constitutive promoter.[33] This genetic circuit was integrated into the chromosomal *urcA* locus and integrates regulatory input from the native, autoregulatory UzcRS and UrpRS TCS, depicted in the gray box. (B) The fluorescence output profile of the core sensor and control variants lacking critical regulatory components over a range of U concentrations. Fluorescence was quantified following a 3 h U exposure as this resulted in the maximal normalized fluorescence signal. Error bars represent the standard deviation of biological triplicates.

Table 1. Hill Function Fitting[a]

sensor variant	half-maximal fluorescence (K)	Hill coefficient	R^2
core sensor	9.9 (0.1)	7.6 (0.3)	0.996
constitutive UzcY	6.3 (0.0)	11.0 (0.6)	1
P_{phyt}-*uzcY*	8.4 (0.1)	9.5 (0.2)	1
UzcRS only	17.4 (0.6)	7.9 (0.3)	0.995
UrpRS only	8.8 (0.7)	12.5 (1.1)	0.999

[a]Parentheses denote the standard deviation of triplicate experiments.

As an alternative approach to improve the coupling and matching of the UzcRS and UrpRS inputs, we considered the use of a signal amplifier module to boost the sensitivity of UzcRS. While the *hrp* (hypersensitive response and pathogenicity) amplifier from *Pseudomonas syringae*[21,38] appeared to be a logical choice given its impressive ability to increase the sensitivity and output dynamic range of the ArsR-based arsenic sensor,[38] we were unable to generate a functional U sensor using *hrpR*, *hrpS*, and P_{hrpL} components in *C. crescentus*. Instead, we leveraged the recently identified membrane protein UzcY that functions as a native signal amplifier for the UzcRS system.[39] Under normal growth conditions, *uzcY* expression is silenced by the MarR family regulator $MarR_1$ (CCNA_03498) and has no effect on UzcRS activity. However, when UzcY expression is induced by deleting $marR_1$, the sensitivity of UzcRS to its metal inducers is enhanced.[39] Deletion of $marR_1$ failed to improve the U sensitivity of UrpRS (Figure S10), suggesting that the U sensitization function of UzcY is specific for UzcRS. The signal amplification mechanism was incorporated within the core sensor by either deleting $marR_1$, which yields a constitutive amplifier function, or by swapping the native *uzcY* promoter with the UrpRS-regulated $P_{phyt\text{-}short}$ (Figure 5A), such that UzcY levels are modulated in a U-concentration dependent manner.

Constitutive UzcY expression significantly enhanced the U sensitivity of the core sensor in the low U concentration range (5−10 μM), yielding a U-dependent fluorescence profile with comparable sensitivity (n^H of 11, K of 6.3 μM; Figure 5B and C; Table 1) to the sensor driven exclusively by UrpRS alone (n^H of 12.5; K of 8.8 μM). A diminished fluorescence output was observed at U concentrations above 10 μM and may reflect reduced tolerance of the $\Delta marR_1$ strain to U toxicity compared to WT as was observed for Zn.[39] Placing *uzcY* under the control of $P_{phyt\text{-}short}$ and, thus, conditionally restricting UzcY function to conditions of UrpRS stimulation, improved sensitivity (n^H of 9.5, K of 8.4) in the 7.5−12.5 μM range, but not to the same degree as constitutive *uzcY* expression (Figure 5B and C). Importantly, neither amplifier configuration altered the Zn-, Cu-, or Pb-dependent induction profile of the core sensor (Figure 5D). By enhancing U sensitivity without affecting Zn sensitivity, the expression of UzcY significantly improved the U to Zn output ratio in the low concentration range (5−10 μM; Figure S9B). Collectively, these data suggest that integration of the UzcRS-specific signal amplifier UzcY overcame the sensitivity limitations of the UzcRS TCS and enhanced the selectivity for U compared to the core sensor. UzcY integration did not correct for the signal amplitude disparity between the core sensor and the sensor driven by UrpRS alone (compare Figure 5B and Figure S7), which was observed at elevated U concentrations (>7.5 μM), likely because the amplitude of the core sensor is limited by the activity of the UzcRS regulated P_{urcB} promoter. This limitation may be at least partially rectified in the UzcY-amplified sensor by swapping P_{urcB} with a promoter that exhibits a higher maximum activity level (e.g., P_{urcA}[27]).

Although the sensor driven by UrpRS alone offers comparable sensitivity and selectivity to the UzcY-amplified core sensor, the use of a combinatorial sensing approach is favored considering the current lack of knowledge on the physiological function of UrpRS and the mechanism governing its U-dependent stimulation. Given the cross-reactivity of UrpRS with Zn and the low concentrations of natural uranium expected in the oligotrophic freshwater environment of this bacterium, we suspect that UrpRS did not evolve to directly detect environmental U, but rather to detect a physiologically relevant stress that is somehow triggered by exposure to U, and to a lesser degree, Zn. As such, it is hypothesized that the inclusion of the UzcRS sensory input within the AND gate sensor will ultimately prove beneficial for minimizing core sensor cross-reactivity with yet unidentified physiological inducers of UrpRS. The successful integration of UzcY within the core sensor enables this selectivity safeguard to be achieved without a trade-off in U sensitivity. The validity of this hypothesis, and the efficacy of UrpRS to function as a standalone U sensor, awaits further characterization of the sensory perception mechanism of both UrpS and UzcS.

Whole-Cell U Sensor Detects as Low as 1.0 μM in Contaminated Groundwater. To test the efficacy of the sensor to detect U in groundwater, samples were collected from wells at three distinct locations at LLNL Site 300, a high-explosives test facility in the Altamont Hills of California, where groundwater concentrations of U may locally exceed the EPA MCL. Quantification of the heavy metal content of each sample

DOI: 10.1021/acssynbio.8b00484
ACS Synth. Biol. 2019, 8, 807−817

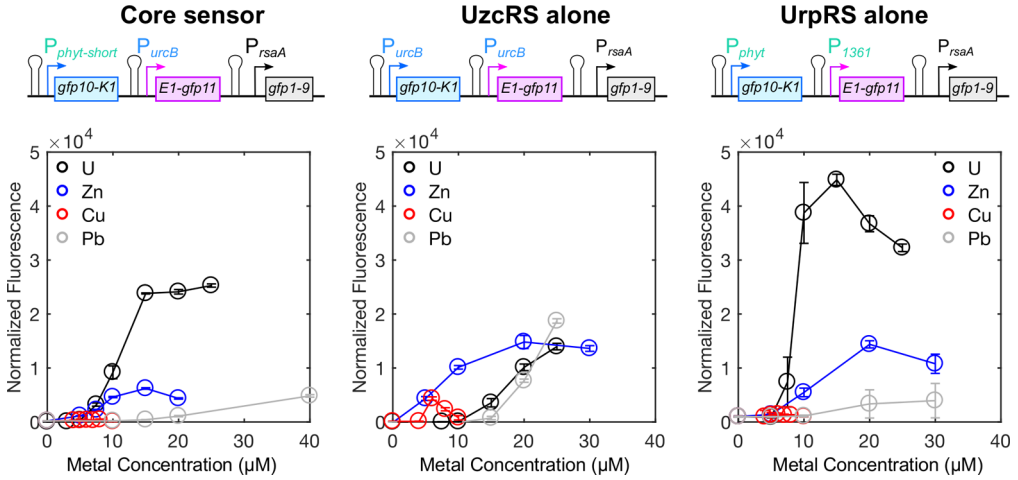

Figure 4. Metal selectivity profile of core sensor and control variants. The top panel depicts simplified schematics of the core sensor and control variants in which the expression of gfp10-K1 and E1-gfp11 components is driven by UzcRS or UrpRS alone. The bottom panel depicts the U/Zn/Cu/Pb response curves for the core sensor and control variants. Fluorescence was quantified following a 3 h exposure to a range of metal concentrations. Error bars represent the standard deviation of biological triplicates.

using ICP-MS or ICP-OES revealed U concentrations that range from 1.0 to 1.24 μM (238−295 ppb; Table 2), representing a challenging test for the whole-cell sensor given the ∼5 μM detection limit observed in M5G G2P medium. Concentrations of the trace metals Zn, Pb, Cu, Cd, and Cr were below detection limits or in the low nanomolar range in all samples (Table 2) and thus not expected to affect sensor performance.

The fluorescence output of the core sensor, UzcY amplifier variants, and negative controls lacking UzcRS, UrpRS, or *gfp1−9* input were monitored as a function of time in the Site 300 samples with and without growth nutrient supplementation. Exposure of the sensor strains to unmodified Site 300 samples yielded no detectable increase in fluorescence and no cell growth (Figure S11; data not shown). In contrast, supplementation with glucose, glycerol-2-phosphate (P source), and ammonium chloride (N source) together, but not glucose alone (data not shown), enabled cell growth and yielded a detectable increase in fluorescence for the core sensor within 6 h of exposure to each sample (Figure 6A). The time course U induction profile of the core sensor was qualitatively similar across each sample with minor differences observed in the signal amplitude (e.g., lower amplitude in sample 2 compared to samples 1 and 3). However, the performance of the signal amplifier strains was more varied. For samples 1 and 3 (∼1 μM U), the $P_{phyt\text{-}short}$-*uzcY* amplifier variant yielded a fluorescence induction profile with slightly lower amplitude compared to the core sensor, while the constitutive amplifier failed to produce an output that differed from the negative controls (Figure 6A). In contrast, in sample 2 (∼1.24 μM U), both signal amplifier variants yielded a fluorescence output signal that exceeded that of the core sensor (Figure 6A), suggesting that UzcRS is limiting U sensor sensitivity in sample 2. This variability in signal amplifier performance between samples may reflect in part a greater susceptibility of strains exhibiting high UzcY expression to environmental stress. Future efforts will seek to optimize the constitutive level of UzcY to improve the performance of this sensor variant in environmental samples. Lastly, compared to the negative controls lacking a UrpR binding site or *gfp1−9* expression, the Δ*uzcR* mutant yielded a fluorescence induction profile with similar kinetics but lower signal amplitude compared to the core sensor. This result suggests that while P_{urcB}-*E1-gfp11* is incompletely insulated from upstream UrpRS-mediated transcriptional activity, the function of both TCS is required to produce the fluorescence response of the core sensor in the groundwater samples.

To further confirm that the fluorescence induction of the core sensor in the groundwater samples was attributed to U, a series of control experiments was performed. A synthetic groundwater sample, which approximated the chemical composition of the Site 300 samples (Table S4), failed to induce core sensor fluorescence in the absence of supplemental U (Figure S12), suggesting that the major element composition of these samples does not induce core sensor fluorescence. Furthermore, the fluorescence induction of the core sensor was significantly reduced in all samples but most prominently in samples 1 and 3, when G2P was replaced with orthophosphate, which reduces U bioavailability (Figure S13). Lastly, uranyl nitrate was added in small, incremental amounts (1 μM increments) to each Site 300 sample, and fluorescence was quantified following a 6 h exposure (Figure 6B). We rationalized that if U is responsible for the fluorescence induction of the whole-cell sensors then small, incremental U additions should further boost sensor fluorescence. A nearly identical linear increase in fluorescence as a function of U concentration was observed for the core sensor in all three groundwater samples, confirming U detectability and further highlighting the consistent U detection performance of the core sensor in the Site 300 samples. The $P_{phyt\text{-}short}$-*uzcY* amplifier variant yielded a comparable U-induction profile as the core sensor in sample 1 but enhanced the signal amplitude for most U concentrations in samples 2 and 3, supporting its ability to increase sensitivity in an environmental context.

Collectively, these data confirm the functionality of the AND gate sensor to detect U in environmental samples and support a lower limit of detection for U of ∼1 μM (∼238 ppb), which is in close agreement with the ∼0.5 μM detection limit reported for the UzcRS-regulated P_{urcA}-*gfpUV* sensor but above the EPA MCL (30 ppb).[26] The detection threshold may be further reduced by rationally tuning the phosphatase activity of UzcS and UrpS, as demonstrated recently for tetrathionate and nitrate sensing TCS,[40] or by increasing U bioavailability through strategic solution conditioning efforts (see discussion below). Nevertheless, the current sensitivity of the AND gate sensor is

DOI: 10.1021/acssynbio.8b00484
ACS Synth. Biol. 2019, 8, 807−817

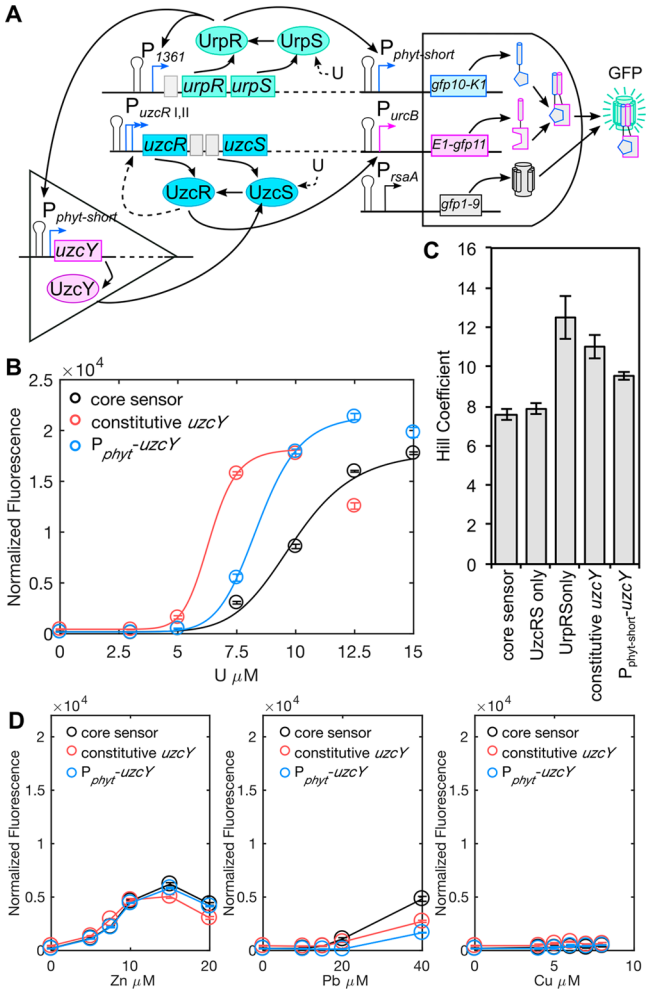

Figure 5. Incorporation of a signal amplifier module within the core sensor circuitry. (A) A schematic for the integration of the UzcY signal amplifier within the U-sensing AND gate. In this variant, *uzcY* is placed under the control of the U-specific promoter $P_{phyt\text{-}short}$ such that the signal amplification is restricted to conditions of U exposure. (B) The fluorescence output of the core sensor and signal amplifier variants following a 3 h exposure to a range of U concentrations. The data were fit with a Hill equation to determine the U concentration that yields half-maximal fluorescence induction and the hill slope as an indicator of U sensitivity. Signal amplifier data points with diminished fluorescence output (i.e., 12.5 μM U for constitutive *uzcY* and 15 μM U for P_{phyt}-*uzcY*) were not included in the curve fitting. (C) Hill coefficients for the signal amplifier strains and the control strains driven by UzcRS and UrpRS alone. (D) The fluorescence output of the core sensor and signal amplifier variants following a 3 h exposure to a range of Zn, Pb, and Cu concentrations. Error bars represent the standard deviation of biological triplicates.

Table 2. Heavy Metal Concentrations in Ground Water Samples

sample site	U (μM)	Zn (nM)	Pb (nM)	Cu (nM)	Cd (nM)	Cr (nM)
Well W-815-2621	1.01 (0.02)	<150	6	13	<9	<19
Well W-812-01	1.24 (0.02)	<150	5	11	<9	<19
Well W-6C	1.09 (0.00)	<150	<5	8	<9	<19

well suited as a screening mechanism (e.g., yes/no) for elevated U concentrations (>200 ppb) in regions with known or suspected anthropogenic contamination or activities. We further anticipate the flexibility to integrate additional analyte-detection modules into the genetic circuitry to enhance the environmental monitoring utility. For example, swapping P_{rsaA} with a promoter responsive to other chemical signatures associated with U enrichment activities would enhance the specificity for U of anthropogenic origin. Additionally, integrating the Zn-responsive, U-independent promoter (e.g., P_{zntA}[27,41]) in an inverted input configuration[42] could minimize false positives attributed to Zn.

The finding that cell growth and U solubility are required for robust U detection has important implications for the environmental application of the sensor. To circumvent the U-phosphate incompatibility, we employed the organophosphate G2P that serves the dual function of providing a phosphate source for cell growth while maintaining initial U solubility through complexation.[24,35] Prior studies have suggested that the physicochemical form—or speciation of U—is dependent on the geochemical conditions and strongly influences bioavailability[1] and consequently the detectability by this biosensor. As such, the successful detection of U in three distinct groundwater samples suggests that the addition of G2P may be a generalizable means of conditioning environmental samples for U detection. Indeed, complexation of uranyl by the G2P isomer glycerol 1-phosphate is expected to dominate U speciation over a wide uranium concentration and pH range.[43] Further investigation of the effect of solution matrix composition on U detectability may unearth additional solution conditioning insights (e.g., other uranyl complexants) to further improve the U detection limit. Given the requirement for nutrient supplementation, we envision that the path toward a fieldable sensor will entail encapsulation of the whole-cell sensor within an integrated detection device that maintains cells in an active state of growth and automates sampling and solution conditioning (e.g., addition of G2P) for detection. Recent efforts have yielded promising results for integrating cell sensors into field-applicable autonomous devices.[10,44,45]

In summary, by identifying and integrating two independent, U-responsive TCS within a synthetic AND gate circuit, a selective U-sensing functionality was developed in *C. crescentus*. The results highlight the value of a combinatorial approach for selective detection of compounds for which there are no known evolved regulators. We expect this approach to be generalizable and drive the development of additional, biobased modules for environmental contaminant detection.

METHODS

Bacterial Strains, Media, and Materials. All strains were derived from wild-type *C. crescentus* strain NA1000 (ATCC 19089) and are listed in Table S6. Cell growth and fluorescence characterization experiments were performed in modified M5G medium (10 mM PIPES, pH 7, 1 mM NaCl, 1 mM KCl, 0.05% NH_4Cl, 0.01 mM Fe/EDTA, 0.2% glucose, 0.5 mM $MgSO_4$, 0.5 mM $CaCl_2$) supplemented with 5 mM glycerol-2-phosphate as the phosphate source (M5G-G2P) to facilitate uranium solubility at the start of growth assays. U stocks were prepared in nitric acid as previously described.[27] A 10 000 ppm $ThCl_4$ stock solution was prepared in 5% nitric acid. Stock solutions of 50−100 mM of $Pb(NO_3)_2$, $NiSO_4$, $ZnCl_2$, $CuSO_4$, $CaCl_2$, $MnCl_2$, $MgSO_4$, K_2CrO_4, Na_2SeO_3, $FeCl_3$, $CoCl_2$, $FeSO_4$, and $NaAsO_2$ were prepared in Milli-Q H_2O, and a 1 g l^{-1} $AlCl_3$ ICP-MS standard in HCl was used for Al addition. All strains were grown at 30 °C with shaking at 220 rpm in Erlenmeyer flasks or

DOI: 10.1021/acssynbio.8b00484
ACS Synth. Biol. 2019, 8, 807−817

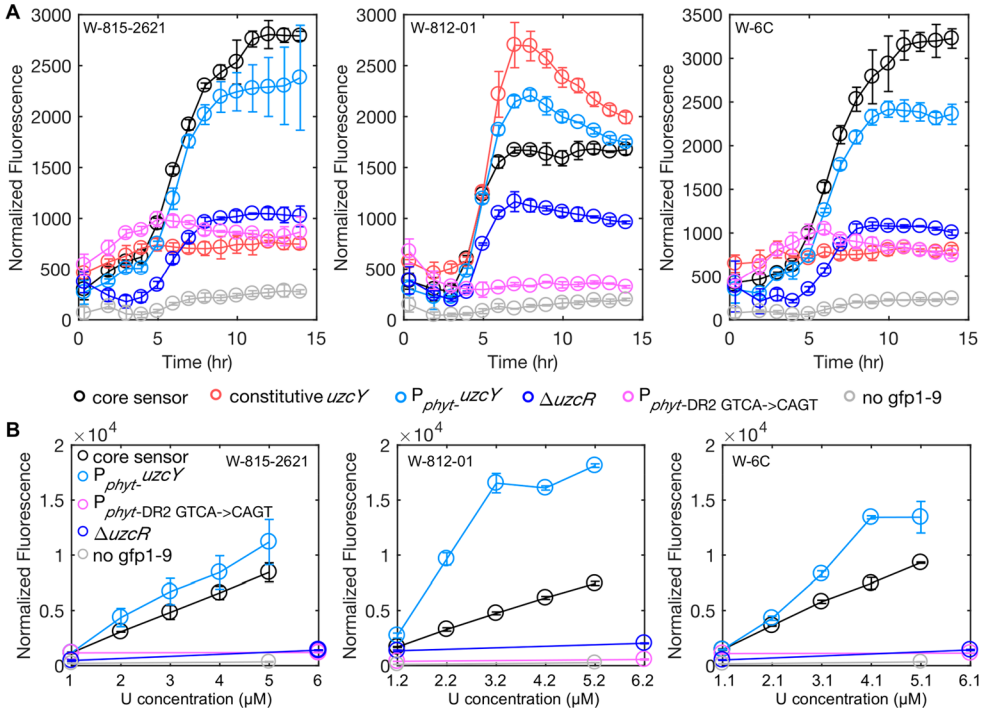

Figure 6. Detection of U in groundwater samples. (A) Fluorescence output of the core sensor and control variants lacking critical regulatory components as a function of time in three distinct Site 300 samples supplemented with glucose (0.2%), glycerol-2-phosphate (5 mM), and ammonium chloride (0.05%). Ground water samples from W-815-2621, W-812-01, and W-6C are referred to as 1, 2, and 3, respectively, in the text. The plot legend is depicted below the plots. (B) The fluorescence of the core sensor and control variants was quantified 6 h after exposure to Site 300 samples supplemented with uranyl nitrate, glucose (0.2%), glycerol-2-phosphate (5 mM), and ammonium chloride (0.05%). The 6 h exposure time was chosen based on the time course fluorescence data presented in panel A. The *x*-axis concentrations represent the total U concentration in the groundwater sample after addition of U in 1 μM increments. Error bars represent the standard deviation of biological triplicates.

at 1000 rpm in 96-well plates in a PHMP-4 Thermoshaker (Grant Instruments). Strain manipulation was performed in PYE medium, containing 0.2% (wt/vol) Bacto peptone (Difco), 0.1% yeast extract (Difco), 1 mM $MgSO_4$, and 0.5 mM $CaCl_2$ and appropriate antibiotics. *Escherichia coli* HST08 (Clontech) was used for cloning following standard procedures.

Clean Deletions and Site-Directed Mutagenesis. In frame deletions of CCNA_01362 and CCNA_01363 were obtained by a two-step *sacB* counterselection procedure[46] as described previously[27] using the primers depicted in Table S5.

Transposon Screen for Regulators of P_{phyt}. A chromosomally integrated P_{phyt}-*lacZ* fusion was constructed using the two-step *sacB* counterselection procedure[46] to swap the P_{urcA} promoter in pDMP82[27] with P_{phyt}. To accomplish this, a P_{phyt} fragment was amplified from the *C. crescentus* genome with the primer pair Phyt-138_F/Phyt-138_R (Table S5) and cloned into pDMP82 that was linearized using the primers 138_PurcA_F and 138_PurcA_F using In-Fusion cloning. The P_{phyt}-*lacZ* fusion was integrated at the chromosomal *urcA* locus in *lacA* mutant strain JOE2321, yielding strain DMP470. For the transposon screen, DMP470 was electroporated with VMCS2::*Tn5Pvan*[47] and plated onto PYE agar plates containing 25 μg mL^{-1} kanamycin. Approximately 12 000 colonies were scraped into a PYE master solution that was frozen and stored at −80 °C. The transposon library was diluted and spread on M5G-G2P agar containing 40 μg mL^{-1} Xgal and 25 μM uranyl nitrate, yielding a total of ∼36 000 colonies. Colonies exhibiting a white colony phenotype were selected, and nested semi-arbitrary PCR was used to map the location of each transposon as described previously.[47]

Construction of Promoter-*gfp* Transcriptional Fusions. Plasmid-borne P_{phyt}-*gfp* and P_{1361}-*gfp* fusions were generated by amplifying P_{phyt} and P_{1361} fragments from the *Caulobacter* genome with the primer pairs *Bam*HI_Pphyt_F /*Eco*RI_Pphyt_R and *Bam*HI_P_{1361}/ *Eco*RI_P_{1361}, respectively, digesting with *Bam*HI and *Eco*RI, and cloning into the similarly digested pDMP450, generating pDMP460 and pDMP463. The promoter-*gfp* fusions were shortened and/or mutated by amplifying pDMP460 and pDMP463 with the primer pairs described in Table S5 and religating using infusion cloning. Mutations were confirmed by sequencing.

Tripartite GFP AND Gate Sensor Construction. A gblock (Tripartite GFP gblock; Table S5) was synthesized (Integrated DNA Technologies) with the following components listed in 5′ to 3′ orientation: promoterless *gfp10-m2_k1*, rrnBT1 and T7Te transcription terminators (BBa_B0015), P_{urcB}-*E1-gfp11-M4*, lamda T_0 terminator, and *gfp1−9* under the control of the *rsaA* promoter (P_{rsaA}[33]). *gfp*10-m2_k1 was placed under the control of P_{phyt} by digesting the Tripartite GFP gblock with *Bgl*II and XhoI and ligating into the similarly digested pDMP460 to form pDMP791. DNA sequence encompassing the entire tripartite DNA and an insulating upstream rrnbT1 transcription terminator was amplified with primers HRP_chrome_int F and HRP_chrome_int R and cloned into pDMP82 that was amplified with the primers urcA_loc_DR_F and urcA-loc_UR_R using infusion cloning to form pDMP792. A variant containing GFP10-m2_k1 under the control of a shortened version of P_{phyt} (i.e., the core sensor) was constructed by amplifying pDMP792 with Pphyt_TR_elim_F and Pphyt_pro-moter_shorten_R and religating using infusion cloning, forming pDMP883. A variant of this AND gate containing gfp1−9 under

DOI: 10.1021/acssynbio.8b00484
ACS Synth. Biol. 2019, 8, 807−817

the control of the xylose inducible promoter (Pxyl[34]) was constructed by amplifying the 360 bp P_{xyl} fragment using Pxyl_F and Pxyl_R and cloning into pDMP792, which was amplified with gfp1−9_amp_for_pxyl_F gfp1−9_amp_for_pxyl_R, using infusion cloning to form pDMP664. All tripartite GFP AND gate variants were then integrated into the chromosomal *urcA* locus using a two-step *sacB* counterselection procedure,[48] forming DMP804, DMP895, and DMP683

A control tripartite variant containing both GFP10-m2_k1 and E1-GFP11-M4 under the control of P_{urcB} was constructed by directionally cloning a P_{urcB} fragment, generated by a XbaI and *Bgl*II digest of the DNA amplied with primers XbaI_PurcB and *Bgl*II_PurcB_R, into the similarly digested pDMP712. Similarly, a tripartite variant containing both GFP10-m2_k1 and E1-GFP11-M4 under the control of UrpRS was constructed by directionally cloning a P_{1361} fragment, generated by a *Kpn*I and AvrII disgest of the DNA amplified with primers *Kpn*I_P_{1361} and AvrII_P_{1361}, into the similarly digested pDMP712. Both control AND gates were cloned into the pNPTS138 double recombination plasmid by amplifying with primers HRP_chrome_int F and HRP_chrome_int R and cloning into pDMP82, which was amplified with the primers urcA_loc_DR_F and urcA-loc_UR_R using Infusion cloning. Finally, the P_{xyl} promoter in both constructs was swapped for P_{rsaA} by cloning P_{rsaA}, amplified with PrsaA_frag_F and PrsaA_frag_R, into the template vectors that were linearized with the primers gfp_for_PrsaA_F and gfp_for_PrsaA_R, forming pDMP932 and pDMP952. These tripartite GFP AND gate variants were then integrated into the chromosomal *urcA* locus to form DMP911 and DMP994.

A U sensing AND gate strain (DMP993) with constitutive UzcY expression was generated by integrating the core sensor (pDMP883) into the *urcA* locus of a strain deleted for CCNA_03498 and CCNA_03499 (DMP863). UzcY expression was restricted to conditions of U exposure by placing *uzcY* expression under the control of $P_{phyt\text{-}short}$ as follows. *uzcY* was amplified from the *C. crescentus* chromosome with primers 3497_for_Pphyt_plas_F and 3497_for_Pphyt_plas_R, digested with *Bgl*II and XhoI, and cloned into the similarly digested pDMP746. The DNA containing the $P_{phyt\text{-}short}$-CCNA_03497 fusion was then amplified with 3497_for_-Pphyt_short_chrome_R and Pphyt_short_for_chrom_3497 and cloned into pDMP1113 that was linearized using the primers chrome_3497_vect_amp_F and chrome_vector_-amp_R. The resulting suicide vector (form pDMP1114) was used to integrate $P_{phyt\text{-}short}$-*uzcY* into DMP993 to form DMP1009.

Metal Induction Experiments. Unless otherwise specified, all metal induction experiments were performed in M5G-G2P. Cells were grown to early exponential phase, washed once with M5G-G2P, and then resuspended in the same volume of fresh M5G-G2P. Washed cells were added in 195 μL aliquots to black 96-well clear bottom plates containing 5 μL of the appropriate metal solution. Cell fluorescence and OD_{600} were determined using a Biotek plate reader (Ex: 480/Em: 516) 2−3 h post-metal exposure. The mean fluorescence and OD_{600} value for each data point was subtracted by the respective values for a M5G-G2P blank, and then the fluorescence was normalized to the OD_{600}. The relationship between the U concentration and the GFP output rate was modeled using a Hill function:

$$y = y_{\min} + \frac{Y_{\max} - Y_{\min}}{1 + \left(\frac{x}{K}\right)^{\eta}}$$

where $y_{\min}$ represents basal normalized fluorescence, $y_{\max}$ is the maximum normalized fluorescence, x represents the U concentration, η is the Hill coefficient, and K is the concentration of U required for half-maximal fluorescence expression. The best fit values were found by using the lsqcurvefit function in Matlab.

Cloning, Overexpression, and Purification of Strep-UrpR. *urpR* was amplified with primers 1362_gene_F and 1362_gene_R_GC and cloned into pET 52-b that was amplified with pET52b_F and pET52b_R using infusion cloning to generate plasmid pDMP1118. *E. coli* BL21(DE3) plys, containing pDMP1118, was grown at 37 °C until an OD_{600} of 0.5 was reached. Isopropyl-1-thio-*b*-D-galactopyranoside (IPTG) was added to 0.5 mM, and the cells were shifted to 30 °C for 4 h of induction. Cells were harvested and stored at −20 °C. The cell pellet was thawed and resuspended in 1.4 mL B-PER Complete Bacterial Protein Extraction Reagent (ThermoFisher), followed by addition of EDTA to 1 mM, and rocking for 15 min at room temperature. Insoluble cell debris was pelleted via centrifugation (20,000xg, 10 min at 4 °C). Strep-UrpR was isolated from cell lysates using a Strep-tactin column as described in the manufacturer's protocol (IBA Lifesciences). The protein concentration of UrpR (reported here as monomers) was determined using a Bradford protein assay (Biorad) with lysozyme as a standard.

Electrophoretic Mobility Shift Assays. A P_{phyt} promoter fragment containing the region from 13 to 245 with respect to the translation initiation site was amplified from pDMP460 and pDMP475 with primers *Bam*HI_Pphyt_F and Pphyt_EMSA_R, the latter of which was labeled with fluorescein on the 5′ end. Prior to the EMSA, the Strep Tag was removed from UzrpR using HRV 3C protease (Thermo Fisher) according to the manufacturer's protocol. UrpR was phosphorylated by incubation in phosphorylation buffer (50 mM Tris, pH 7.9, 150 mM NaCl, 10 mM $MgCl_2$) with 50 mM disodium carbamyl phosphate (Sigma-Aldrich) for 1 h at 30 °C and immediately used in the binding assays. EMSAs were performed by incubating phosphorylated UrpR with P_{phyt} DNA (50 nM) for 10 min at 37 °C in buffer containing 50 mM Tris−HCl (pH 7.9), 200 mM NaCl, 10 mM $MgCl_2$, 0.1 mg mL^{-1} BSA, 5% glycerol, 1 mM DTT, and 50 μg mL^{-1}poly-dI-dC. A 5% TBE mini-protean polyacrylamide gel was pre-run with 0.5× TBE at 120 V for 30 min in a Mini-PROTEAN tetra cell (Bio-Rad) prior to loading samples. Samples were run at 100 V for 45 min, and the reaction products were visualized using a Biorad Gel Doc XR1 System.

Site 300 Sample Collection. Standard operating procedures for sampling and sample handling at LLNL Site 300 have been described in detail[49] and are consistent with the guidance and requirements of the United States Environmental Protection Agency. The groundwater samples used in this study were collected from each well with either an electrical submersible pump or a bailer. Well samples were placed on ice, filtered using a 0.2 μm filter, and stored at 4 °C.

Inductively Coupled Plasma Mass Spectrometry/Optical Emission Spectrometry. Site 300 samples were diluted in 2% (v/v) nitric acid (trace metal grade) and spiked with an internal holmium standard. U was quantified using a Thermo XSeriesII ICP-MS run in standard mode. The sample introduction system was an ESI PFA-ST nebulizer pumped at

DOI: 10.1021/acssynbio.8b00484
ACS Synth. Biol. 2019, 8, 807−817

120 μL/min. Zn, Pb, Cu, Cd, and Cr were quantified using a Thermo iCAP 7400 radial ICP-OES in standard operating mode. Standard curves were generated using a 100 mM uranyl nitrate stock solution and 10 ppm Zn, Pb, Cu, Cd, and Cr ICP-MS standards (Inorganic Ventures).

■ ASSOCIATED CONTENT

Supporting Information

The Supporting Information is available free of charge on the ACS Publications website at DOI: 10.1021/acssynbio.8b00484.

Figure S1, identification of a U responsive promoter element in *C. crescentus*; Figure S2, transposon insertions within CCNA_01362 and CCNA_01363 abrogate U-dependent induction of P_{phyt}; Figure S3, functional independence and metal selectivity of UrpRS and UzcRS; Figure S4, schematic of U-sensing AND gate configurations used in this study; Figure S5, U sensing AND gate variants with different mechanisms of gfp1−9 expression; Figure S6, core sensor is not responsive to nitrate; Figure S7, U response curves for the core sensor and control variants in which the expression of gfp10-K1 and E1-gfp11 components is driven by UzcRS or UrpRS alone; Figure S8, metal selectivity profile of core sensor; Figure S9, zoomed-in version of the U/Zn/Cu/Pb response curves for the core sensor, control variants, and *uzcY* amplifier variants; Figure S10, constitutive UzcY expression does not improve the U sensitivity of UrpRS; Figure S11, fluorescence output of sensor variants in groundwater samples without nutrient supplementation; Figure S12, fluorescence output of sensor variants in synthetic groundwater samples; Figure S13, fluorescence output of sensor variants groundwater samples with orthophosphate in place of G2P (PDF)

Table S1, fold change in CCNA_01361 and CCNA_01362 expression under various stress conditions; Table S2, transposons in CCNA_01362 and CCNA_01363 that abolished U-dependent induction of P_{phyt}-*lacZ*; Table S3, metal selectivity of UrpRS and UzcRS; Table S4, chemical composition of Site 300 and synthetic groundwater samples; Table S5, primers and gblocks used in this study; Table S6, strains and plasmids (XLSX)

■ AUTHOR INFORMATION

Corresponding Author

*E-mail: park36@llnl.gov; Phone: +1-925-423-7508.

ORCID

Dan M. Park: 0000-0002-6000-6805

Notes

The authors declare no competing financial interest.

■ ACKNOWLEDGMENTS

We thank Mimi Yung, K. Wes Overton, and Tek Hyung Lee for critical reading of this manuscript. This work was performed under the auspices of the U.S. Department of Energy by Lawrence Livermore National Laboratory under Contract DE-AC52-07NA27344 (LLNL-JRNL-760180). This study was supported by the Laboratory Directed Research and Development Program at Lawrence Livermore National Laboratory (LDRD# 16-LW-055).

■ REFERENCES

(1) Markich, S. J. (2002) Uranium speciation and bioavailability in aquatic systems: an overview. *Sci. World J. 2*, 707−729.

(2) Brugge, D., and Buchner, V. (2011) Health effects of uranium: new research findings. *Rev. Environ. Health 26*, 231−249.

(3) Nolan, J., and Weber, K. A. (2015) Natural Uranium Contamination in Major U.S. Aquifers Linked to Nitrate. *Environ. Sci. Technol. Lett. 2*, 215−220.

(4) Focazio, M. J., Tipton, D., Shapiro, S. D., and Geiger, L. H. (2006) The chemical quality of self-supplied domestic well water in the United States. *Groundwater Monit. Rem. 26*, 92−104.

(5) Hoover, J., Gonzales, M., Shuey, C., Barney, Y., and Lewis, J. (2017) Elevated Arsenic and Uranium Concentrations in Unregulated Water Sources on the Navajo Nation, USA. *Exposure Health 9*, 1−12.

(6) Wang, F., Chen, Y., Zhao, Y.-g., Zhang, Y., Wang, T.-x., Li, J.-h., Chang, Z.-y., and Cui, H.-p. (2013) Primary studies on particle recovery of swipe samples for nuclear safeguards. *J. Radioanal. Nucl. Chem. 298*, 1865−1869.

(7) Park, M., Tsai, S. L., and Chen, W. (2013) Microbial biosensors: engineered microorganisms as the sensing machinery. *Sensors 13*, 5777−5795.

(8) Yagi, K. (2007) Applications of whole-cell bacterial sensors in biotechnology and environmental science. *Appl. Microbiol. Biotechnol. 73*, 1251−1258.

(9) Bereza-Malcolm, L. T., Mann, G., and Franks, A. E. (2015) Environmental sensing of heavy metals through whole cell microbial biosensors: a synthetic biology approach. *ACS Synth. Biol. 4*, 535−546.

(10) Truffer, F., Buffi, N., Merulla, D., Beggah, S., van Lintel, H., Renaud, P., van der Meer, J. R., and Geiser, M. (2014) Compact portable biosensor for arsenic detection in aqueous samples with *Escherichia coli* bioreporter cells. *Rev. Sci. Instrum. 85*, 015120.

(11) Hwang, I. Y., Koh, E., Wong, A., March, J. C., Bentley, W. E., Lee, Y. S., and Chang, M. W. (2017) Engineered probiotic Escherichia coli can eliminate and prevent Pseudomonas aeruginosa gut infection in animal models. *Nat. Commun. 8*, 15028.

(12) King, J. M., Digrazia, P. M., Applegate, B., Burlage, R., Sanseverino, J., Dunbar, P., Larimer, F., and Sayler, G. S. (1990) Rapid, sensitive bioluminescent reporter technology for naphthalene exposure and biodegradation. *Science 249*, 778−781.

(13) Belkin, S., Yagur-Kroll, S., Kabessa, Y., Korouma, V., Septon, T., Anati, Y., Zohar-Perez, C., Rabinovitz, Z., Nussinovitch, A., and Agranat, A. J. (2017) Remote detection of buried landmines using a bacterial sensor. *Nat. Biotechnol. 35*, 308−310.

(14) Kabessa, Y., Eyal, O., Bar-On, O., Korouma, V., Yagur-Kroll, S., Belkin, S., and Agranat, A. J. (2016) Standoff detection of explosives and buried landmines using fluorescent bacterial sensor cells. *Biosens. Bioelectron. 79*, 784−788.

(15) Liu, J., Brown, A. K., Meng, X., Cropek, D. M., Istok, J. D., Watson, D. B., and Lu, Y. (2007) A catalytic beacon sensor for uranium with parts-per-trillion sensitivity and millionfold selectivity. *Proc. Natl. Acad. Sci. U. S. A. 104*, 2056−2061.

(16) Xiao, S. J., Zuo, J., Zhu, Z. Q., Ouyang, Y. Z., Zhang, X. L., Chen, H. W., and Zhang, L. (2015) Highly sensitive DNAzyme sensor for selective detection of trace uranium in ore and natural water samples. *Sens. Actuators, B 210*, 656−660.

(17) Blake, I. R., Pavlov, A. R., Khosraviani, M., Ensley, H. E., Kiefer, G. E., Yu, H., Li, X., and Blake, D. A. (2004) Novel monoclonal antibodies with specificity for chelated uranium(VI): isolation and binding properties. *Bioconjugate Chem. 15*, 1125−1136.

(18) Quesada-González, D., Jairo, G. A., Blake, R. C., Blake, D. A., and Merkoçi, A. (2018) Uranium (VI) detection in groundwater using a gold nanoparticle/paper-based lateral flow device. *Sci. Rep. 8*, 16157.

(19) Wegner, S. V., Boyaci, H., Chen, H., Jensen, M. P., and He, C. (2009) Engineering a uranyl-specific binding protein from NikR. *Angew. Chem., Int. Ed. 48*, 2339−2341.

(20) Wang, B., Barahona, M., and Buck, M. (2013) A modular cell-based biosensor using engineered genetic logic circuits to detect and integrate multiple environmental signals. *Biosens. Bioelectron. 40*, 368−376.

DOI: 10.1021/acssynbio.8b00484
ACS Synth. Biol. 2019, 8, 807−817

(21) Wang, B., Kitney, R. I., Joly, N., and Buck, M. (2011) Engineering modular and orthogonal genetic logic gates for robust digital-like synthetic biology. *Nat. Commun. 2*, 508.
(22) Clarke, E. J., and Voigt, C. A. (2011) Characterization of combinatorial patterns generated by multiple two-component sensors in *E. coli* that respond to many stimuli. *Biotechnol. Bioeng. 108*, 666−675.
(23) Hu, P., Brodie, E. L., Suzuki, Y., McAdams, H. H., and Andersen, G. L. (2005) Whole-genome transcriptional analysis of heavy metal stresses in *Caulobacter crescentus*. *J. Bacteriol. 187*, 8437−8449.
(24) Park, D. M., and Jiao, Y. (2014) Modulation of medium pH by *Caulobacter crescentus* facilitates recovery from uranium-induced growth arrest. *Appl. Environ. Microbiol. 80*, 5680−5688.
(25) Yung, M. C., Ma, J., Salemi, M. R., Phinney, B. S., Bowman, G. R., and Jiao, Y. (2014) Shotgun proteomic analysis unveils survival and detoxification strategies by *Caulobacter crescentus* during exposure to uranium, chromium, and cadmium. *J. Proteome Res. 13*, 1833−1847.
(26) Hillson, N. J., Hu, P., Andersen, G. L., and Shapiro, L. (2007) *Caulobacter crescentus* as a whole-cell uranium biosensor. *Appl. Environ. Microbiol. 73*, 7615−7621.
(27) Park, D. M., Overton, K. W., Liou, M. J., and Jiao, Y. (2017) Identification of a U/Zn/Cu responsive global regulatory two-component system in *Caulobacter crescentus*. *Mol. Microbiol. 104*, 46−64.
(28) Cabantous, S., Nguyen, H. B., Pedelacq, J. D., Koraichi, F., Chaudhary, A., Ganguly, K., Lockard, M. A., Favre, G., Terwilliger, T. C., and Waldo, G. S. (2013) A new protein-protein interaction sensor based on tripartite split-GFP association. *Sci. Rep. 3*, 2854.
(29) Blanco, A. G., Sola, M., Gomis-Rüth, F. X., and Coll, M. (2002) Tandem DNA Recognition by PhoB, a Two-Component Signal Transduction Transcriptional Activator. *Structure 10*, 701−713.
(30) Park, D. M., and Kiley, P. J. (2014) The influence of repressor DNA binding site architecture on transcriptional control. *mBio 5*, e01684.
(31) Nriagu, J. O. (1972) Lead orthophosphates. I. Solubility and hydrolysis of secondary lead orthophosphate. *Inorg. Chem. 11*, 2499−2503.
(32) Tripet, B., Yu, L., Bautista, D. L., Wong, W. Y., Irvin, R. T., and Hodges, R. S. (1997) Engineering a de novo designed coiled-coil heterodimerization domain for the rapid detection, purification and characterization of recombinantly expressed peptides and proteins. *Protein Eng., Des. Sel. 10*, 299.
(33) Fisher, J. A., Smit, J., and Agabian, N. (1988) Transcriptional analysis of the major surface array gene of Caulobacter crescentus. *J. Bacteriol. 170*, 4706−4713.
(34) Meisenzahl, A. C., Shapiro, L., and Jenal, U. (1997) Isolation and characterization of a xylose-dependent promoter from *Caulobacter crescentus*. *J. Bacteriol. 179*, 592−600.
(35) Yung, M. C., and Jiao, Y. (2014) Biomineralization of uranium by PhoY phosphatase activity aids cell survival in *Caulobacter crescentus*. *Appl. Environ. Microbiol. 80*, 4795−4804.
(36) National Research, C. (1977) *Drinking Water and Health*, Vol. *1*, The National Academies Press, Washington, DC.
(37) Pieper, K. J., Krometis, L.-A. H., Gallagher, D. L., Benham, B. L., and Edwards, M. (2015) Incidence of waterborne lead in private drinking water systems in Virginia. *J. Water Health 13*, 897−908.
(38) Wang, B., Barahona, M., and Buck, M. (2014) Engineering modular and tunable genetic amplifiers for scaling transcriptional signals in cascaded gene networks. *Nucleic Acids Res. 42*, 9484−9492.
(39) Park, D. M., Wesley Overton, K., and Jiao, Y. (2018) The UzcRS two-component system in Caulobacter crescentus integrates regulatory input from diverse auxiliary regulators. *Mol. Microbiol.*, DOI: 10.1111/mmi.14180.
(40) Landry, B. P., Palanki, R., Dyulgyarov, N., Hartsough, L. A., and Tabor, J. J. (2018) Phosphatase activity tunes two-component system sensor detection threshold. *Nat. Commun. 9*, 1433.
(41) Mazzon, R. R., Braz, V. S., da Silva Neto, J. F., and do Valle Marques, M. (2014) Analysis of the *Caulobacter crescentus* Zur regulon reveals novel insights in zinc acquisition by TonB-dependent outer membrane proteins. *BMC Genomics 15*, 734.
(42) Wang, B., and Buck, M. (2014) Rapid engineering of versatile molecular logic gates using heterologous genetic transcriptional modules. *Chem. Commun. 50*, 11642−11644.
(43) Koban, A., and Bernhard, G. (2004) Complexation of uranium(VI) with glycerol 1-phosphate. *Polyhedron 23*, 1793−1797.
(44) Roggo, C., and van der Meer, J. R. (2017) Miniaturized and integrated whole cell living bacterial sensors in field applicable autonomous devices. *Curr. Opin. Biotechnol. 45*, 24−33.
(45) Buffi, N., Beggah, S., Truffer, F., Geiser, M., van Lintel, H., Renaud, P., and van der Meer, J. R. (2016) An automated microreactor for semi-continuous biosensor measurements. *Lab Chip 16*, 1383−1392.
(46) Stephens, C., Reisenauer, A., Wright, R., and Shapiro, L. (1996) A cell cycle-regulated bacterial DNA methyltransferase is essential for viability. *Proc. Natl. Acad. Sci. U. S. A. 93*, 1210−1214.
(47) Christen, B., Fero, M. J., Hillson, N. J., Bowman, G., Hong, S. H., Shapiro, L., and McAdams, H. H. (2010) High-throughput identification of protein localization dependency networks. *Proc. Natl. Acad. Sci. U. S. A. 107*, 4681−4686.
(48) Fiebig, A., Castro Rojas, C. M., Siegal-Gaskins, D., and Crosson, S. (2010) Interaction specificity, toxicity and regulation of a paralogous set of ParE/RelE-family toxin-antitoxin systems. *Mol. Microbiol. 77*, 236−251.
(49) Goodrich, R., and Lorega, G. (2016) *LLNL Livermore Site and Site 300 Environmental Restoration Project Standard Operating Procedures (SOPs)*, Lawrence Livermore National Laboratory, Livermore, California (UCRL-MA-109115 Rev. 15).

DOI: 10.1021/acssynbio.8b00484
ACS Synth. Biol. 2019, 8, 807−817